ORGANIC CHEMISTRY

FRONTIERS

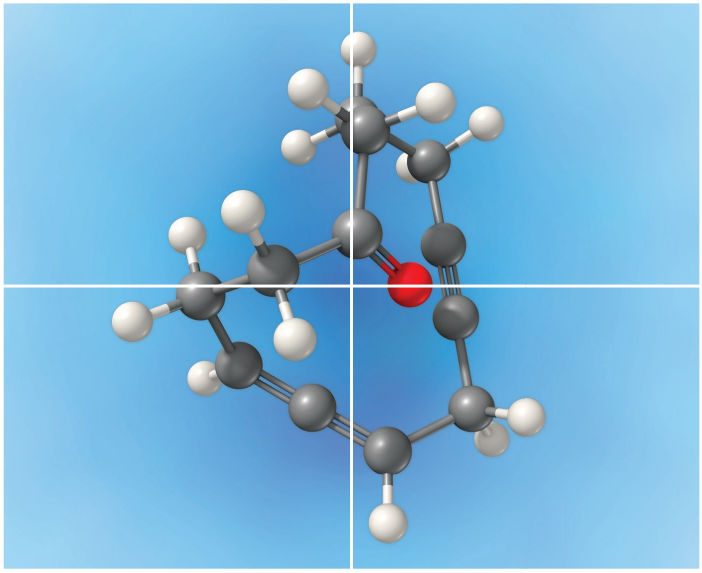

Accepted Manuscript

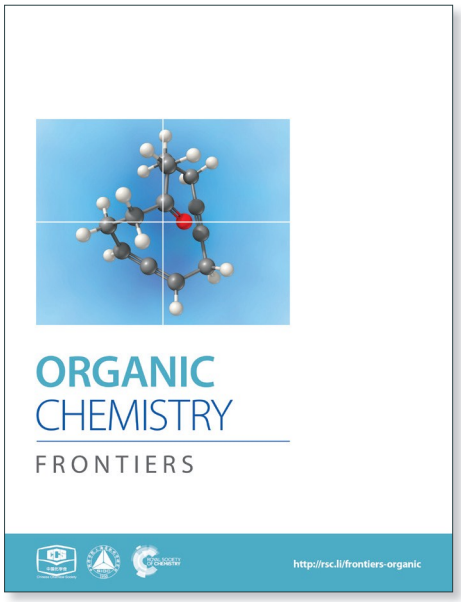

This is an *Accepted Manuscript*, which has been through the Royal Society of Chemistry peer review process and has been accepted for publication.

Accepted Manuscripts are published online shortly after acceptance, before technical editing, formatting and proof reading. Using this free service, authors can make their results available to the community, in citable form, before we publish the edited article. We will replace this *Accepted Manuscript* with the edited and formatted *Advance Article* as soon as it is available.

You can find more information about *Accepted Manuscripts* in the **Information for Authors**.

Please note that technical editing may introduce minor changes to the text and/or graphics, which may alter content. The journal's standard **Terms & Conditions** and the **Ethical guidelines** still apply. In no event shall the Royal Society of Chemistry be held responsible for any errors or omissions in this *Accepted Manuscript* or any consequences arising from the use of any information it contains.

DFT perspective toward [3 + 2] annulation reaction of enals with α-ketoamides through NHC and Brønsted acid cooperative catalysis: mechanism, stereoselectivity, and role of NHC

Yang Wang, Bohua Wu, Linjie Zheng, Donghui Wei*, and Mingsheng Tang*

The College of Chemistry and Molecular Engineering, Center of Computational Chemistry, Zhengzhou University, Zhengzhou, Henan Province, 450001, P.R. China

Abstract

A systematic theoretical study has been carried out to understand the possible mechanisms and stereoselectivity of the N-heterocyclic carbene (NHC)-catalyzed [3 + 2] annulation reaction of enals with α-ketoamides using the density functional theory (DFT) calculations. The calculated results reveal that the favorable pathway comprises of seven steps, *i.e.*, addition of the catalyst, formation of Breslow intermediate, formation of enolate intermediate, C–C bond formation step, proton transfer process, ring-closure process and the regeneration of the catalyst. For the proton transfer process, apart from the direct proton transfer mechanism, the base TMEDA and the *in situ* generated Brønsted Acid TMEDA·H^+ mediated proton transfer mechanisms are also investigated; the free energy for the curial proton transfer steps is found to be significantly lowered by explicit inclusion of the Brønsted Acid TMEDA·H^+. The computational results show that the C–C bond formation step is the stereoselectivity-determining step, in which two chirality centers assigned on the coupling carbon atoms are formed, and the RR-configured diastereomer is the predominant product, which is in good agreement with the experimental observations. Global reaction index (GRI) analysis has been performed to confirm that NHC mainly plays a role of Lewis base catalyst. In addition, the distortion/interaction, NCI, and NBO analyses show that the strong interaction and electron delocalization of the reaction active site determine the stereoselectivity, with RR-configured product being generated preferentially. The mechanistic insights obtained in the present study should be valuable for the rational design of effective organocatalyst for this kind of reaction with high stereoselectivity.

Keywords: N-heterocyclic carbene, [3 + 2] annulation, Cooperative catalysis

* Corresponding authors: donghuiwei@zzu.edu.cn (D. H. Wei) and mstang@zzu.edu.cn (M. S. Tang)

1. Introduction

During the past decades, N-heterocyclic carbenes (NHC) have been widely applied in organic chemistry.[1] As an important organocatalysts, NHCs have been successfully used in carbon-carbon and carbon-heteroatom bond formation reactions including cross-benzion, Stetter, homoenolate, cycloaddition, and annulation reactions, and so on.[2] Specially, the NHC catalysis has emerged as a powerful tool for the development of new transformations to construct heterocycles with high stereoselectivity and regioselectivity. Owing to the unique properties of NHC catalysts, a huge amount of advances continue to be made. For example, various types of ketene cycloaddition reactions, including the [2 + 2],[2c,2j,3] [2 + 2 + 2],[3c,4] and [4 + 2][5] cycloaddition reactions with high stereoselectivity, are reported by Ye's group for the construction of N/O-containing heterocycles.

Recently, several types of the NHC catalyzed annulation reactions between enals and the different electrophilic coupling partners, such as alkenes, imines, and ketones have attracted more and more attention. Interestingly, the addition of the NHC catalyst to the enals can allow the inversion of the normal reactivity (i.e. umpolung) through formation of Breslow intermediates (**Scheme 1a**) and serve as the prenucleophiles, which then will lead to different reactive intermediates bearing more than one reactive carbon center of the enals, such as the *β*-carbon (homoenolate intermediate, **Scheme 1b**),[2k,6] *α*-carbon (enolate intermediate, **Scheme 1c**),[7] γ-carbon (dienolate intermediate, **Scheme 1d**),[2b,8] and carbonyl carbon (acyl anion equivalent intermediate, **Scheme 1e**).[9] As shown in **Scheme 1**, the Breslow intermediates can be employed as the one-, two-, three-, and four-carbon synthons in the different annulations reactions. For example, the cross-benzion reaction undergoes when the Breslow intermediate works as the C1-synthon (**Scheme 1e**)[9]. When they function as two-, three-, and four-carbon synthons, various types of annulation reactions including [2 + 4],[2i,10] [3 + n] (n=2, 3, 4),[2d,2e,2g,2h,6e,11] and [4 + n] (n=2, 3)[6d,12] annulation reactions, then occur under the NHC catalysis. Most of the reported NHC-catalyzed [3 + 2] annulations reactions of enals between enals and C=X bonds (X=O, NR, and CHR) involve a homoenolate intermediate (**Scheme 1b**), while the NHC-catalyzed [3 + 2] annulation via azolium enolate intermediates (**Scheme 1c**) has been less studied. Recently, an outstanding work on the first example of the NHC-catalyzed [3 + 2] annulation reaction of *α*,*β*-unsaturated aldehydes (enals) with *α*-ketoamides (**Scheme 2**) was reported by Enders and co-authors.[13] It should be noted that no other group has focused on applying the azolium enolate strategy in order to synthesize

useful heterocycles by the NHC-catalyzed [3 + 2] annulation reactions, indicating a unique propensity in azolium enolate chemistry is to give useful heterocycles or natural products.

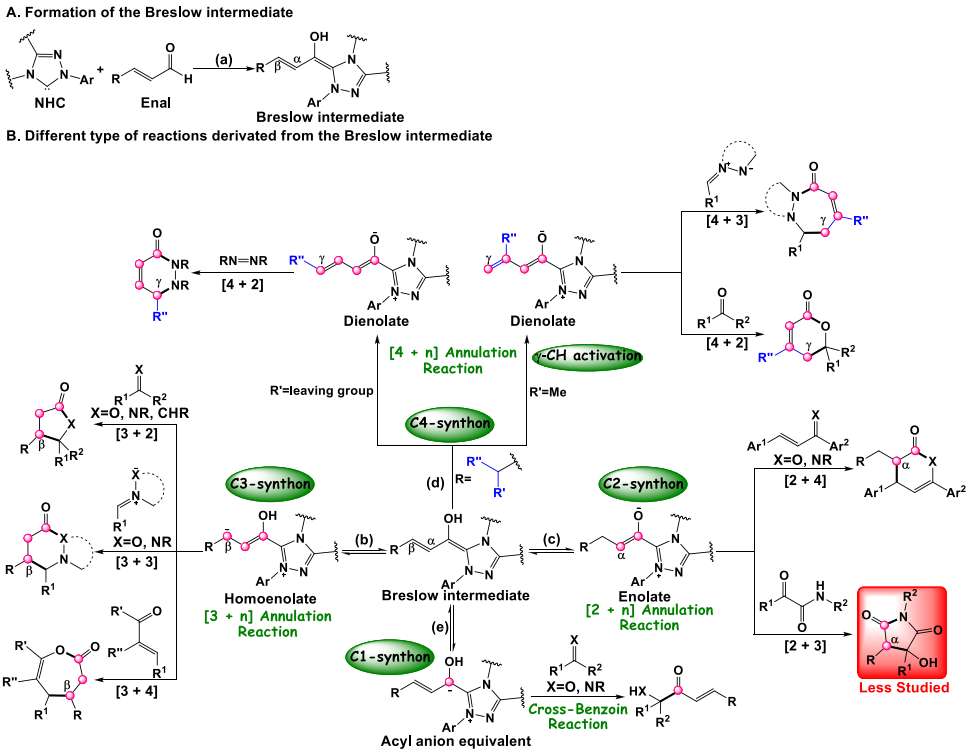

Scheme 1 NHC catalyst-controlled formation of different reactive intermediates from enals.

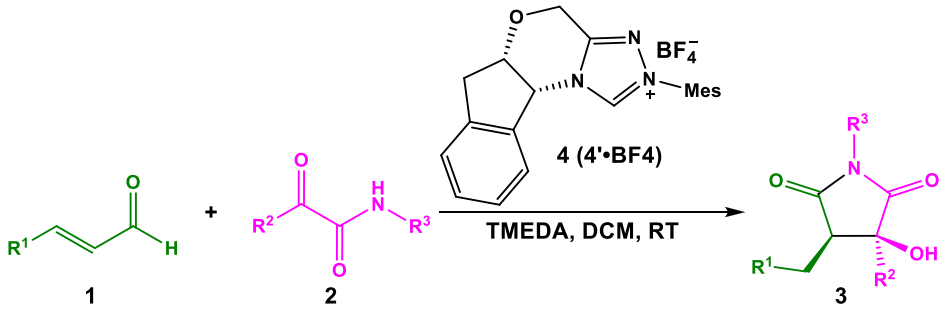

Scheme 2 NHC-catalyzed [3 + 2] annulation reaction of enals with α-ketoamides.

Accompanied with the great development of NHC-catalyzed annulation reactions of enals in experiment, the theoretical investigations on the detailed mechanisms have also been reported in the literatures. For example, Bode and co-workers computationally studied the NHC-catalyzed [4 + 2] annulation reaction of *α,β*-unsaturated aldehydes with enones via the enolate intermediate, they indentified that the oxyanion-steering mechanism and CH-π interaction are the two crucial interactions for the high selectivity.[14] Our group has performed the theoretical investigation on the

mechanism of the NHC-catalyzed [4 + 2] annulation reaction of enals via the enolate or dienolate intermediates, and the computational results show that the acetic acid or the *in situ* formed acid can assist the proton transfer process.[15] Sunoj et al. performed a series of theoretical investigations on the mechanism and enantioselectivity of NHC-catalyzed Stetter reaction and annulation reactions of enals via the homoenolate intermediate.[16] More recently, we have also studied the annulation reaction of allenals with chalcones catalyzed by NHC, in which the origin of the unexpected chemoselectivity has been disclosed.[17] Moreover, the mechanisms and stereoselectivities of the NHC-catalyzed ketene cycloaddition reactions (including [2 + 2],[18] [2 + 2 + 2],[19] and [4 + 2] cycloaddition reactions[20]) have also been investigated by our group. These theoretical studies have greatly enhanced our understanding of the mechanistic insights into the NHC catalysis. Noteworthy, the reaction mechanism might be diverse for different NHC catalytic annulation reactions of enals, because the catalysts, reactants, and additives will influence the proton transfer process involved in these kinds of reactions. Thus, the theoretical investigation is necessary for these special organocatalytic reactions.

As mentioned above, **Scheme 2** illustrates the experimental details of the NHC-catalyzed [3 + 2] annulation reaction of enals with *α*-ketoamides: enal **1** reacts with α-ketoamide **2** to give the desired five-membered heterocyclic compound **3** catalyzed by NHC **4'** with the presence of TMEDA using DCM as the solvent, which is generated from the triazolium salt **4** at room temperature. As shown in **Scheme 3**, Enders and co-workers have conducted some efforts to propose the possible reaction mechanism in experiment, their explorations for this novel reaction are quite instructive, but there still are some key issues that need to be settled: (1) In the second step, the direct [1, 2]-proton transfer process for the formation of Breslow intermediate would cost quite high energy barrier due to the large strain in the three-membered ring transition state. Moreover, the reaction proceeds without a protic additive in the reaction system, so how does the [1, 2]-proton transfer process happen? (2) What are the roles of the NHC catalyst and the base TMEDA? (3) As a design of a new organocatalyst relies on a detailed understanding of the underlying factors that govern the stereoselectivity of these kinds of reactions, so what are the key factors on controlling the stereoselectivity of this reaction? To the best of our knowledge, the computational investigation on the detailed mechanism and stereoselectivity of NHC-catalyzed [3 + 2] annulation reaction of enals with *α*-ketoamides remains to be unexplored to date. Our

interests in the NHC catalysis promotes us to pursue a theoretical investigation on the title reaction to not only obtain a preliminary picture from the α,β-unsaturated aldehyde [3 + 2] annulation reaction, but also explore the factors that govern the stereochemistry of this reaction. We believe that the mechanistic information should be important for understanding the NHC-catalyzed [3 + 2] annulation reactions and providing novel insights into recognizing this kind of reaction in detail.

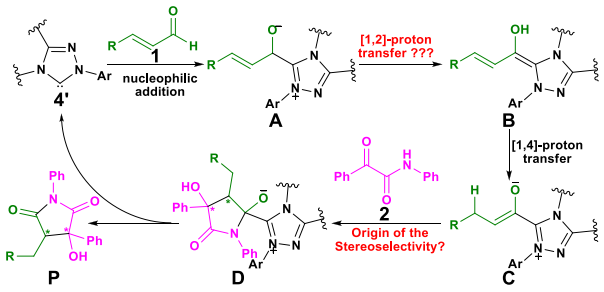

Scheme 3 The proposed catalytic cycle of the NHC-catalyzed [3 + 2] annulation reaction.

As depicted in **Scheme 2**, the [3 + 2] annulation reaction between the enal with R^1=Ph (denoted as **R1**) and α-ketoamide with R^2=R^3=Ph (denoted as **R2**) catalyzed by the active NHC catalyst **4'** (denoted as **Cat**) for the formation of N-heterocyclic product, in which obtains the high yields (83%) with excellent enantioselectivities (99%) and very good diastereoselectivities (>20:1), has been chosen as the model reaction to investigate the detailed mechanism and stereoselectivity for this kind of reactions using density functional theory.

2. Computational Details

Quantum mechanical calculations reported herein were carried out with the Gaussian 09 suite of programs[21] by using density functional theory, which has been revealed to be a powerful tool for clarifying the detailed reaction mechanisms and predicting the stereoselectivity as well as chemoselectivity in both organic, biological reactions, and so on.[22] The solution-phase geometry optimization of all species is performed with the recently developed M06-2X[23] density functional along with the 6-31G(d, p) basis set in DCM solvent using the integral equation formalism polarizable continuum model (IEF-PCM).[24] The harmonic vibrational frequency calculations were performed at the same level of theory as that used for geometry optimizations to provide thermal corrections of Gibbs free energies and make sure that the local minima had no imaginary frequencies, while the saddle points had only one imaginary frequency. Intrinsic reaction

coordinates (IRCs)[25] were calculated to confirm that the transition state structure connected the correct reactant and product on the potential energy surface. The natural bond orbital (NBO)[26] analysis was employed to assign the atomic charges. Non-covalent interactions (NCIs) analysis was plotted using Multiwfn (version 3.3.8).[27] The computed structures were rendered using the CYLView software.[28] We choose to discuss the calculated results based on the solution-phase Gibbs free energies obtained at the M06-2X/6-31G(d, p)/IEF-PCM$_{(DCM)}$ level.

To test the accuracy of the M06-2X/6-31G(d, p)//IEF-PCM$_{DCM}$ level, we have performed the single-point energy calculations for the key transition states by using the higher basis sets, i.e. M06-2X/6-311++G(2df, 2pd)//IEF-PCM$_{DCM}$, M06-2X/6-311++G(2df, 2pd)//SMD$_{DCM}$, ωB97X-D[29]/6-311++G(2df, 2pd)//IEF-PCM$_{DCM}$, and ωB97X-D/6-311++G(2df, 2pd)//SMD$_{DCM}$, and the computed single-point energies with the zero-point and thermal corrections calculated at the M06-2X/6-31G(d, p)//IEF-PCM$_{DCM}$ level were summarized in **Table S1** of electronic supplementary information (ESI). Further, we have additionally optimized the geometries and calculated the free energies of reactants, catalyst, and the stationary points involved in the stereoselectivity-determining step at the M06-2X/6-31G(d, p)//SMD$_{DCM}$, ωB97X-D/6-31G(d, p)//IEFPCM$_{DCM}$, and ωB97X-D/6-31G(d, p)//SMD$_{DCM}$ levels, which have been summarized in **Table S2** of ESI. The computational outcomes show that the free energies calculated at the M06-2X/6-31G(d, p)//IEF-PCM$_{DCM}$ level has the same trend and small differences with those calculated at the different levels mentioned above, indicating the selected M06-2X functional, 6-31G(d, p) basis set, and IEF-PCM solvation model is suitable and reliable for studying the NHC-catalyzed [3 + 2] annulation reaction.

3. Results and Discussion

3.1. Reaction Mechanisms

In this part, the detailed mechanisms of enals (**R1**) with *α*-ketoamides (**R2**) catalyzed by NHC have been studied and discussed intensively. As shown in **Scheme 4**, we suggested the possible catalytic cycle which comprises of seven reaction steps, *i.e.* the addition of the catalyst **Cat** to the Re/Si-face of **R1** for the formation of the zwitterionic intermediate **Re/Si-M1** via transition state **Re/Si-TS1**, the [1, 2]-proton transfer process to generate the Breslow intermediate **Re/Si-M2** via transition state **Re/Si-TS2**, the [1, 4]-proton transfer process for the formation of the

azolium enolate intermediate **Re/Si-M3** via transition state **Re/Si-TS3**, addition of another reaction pattern **R2** to give zwitterionic intermediate **M4RR/RS/SR/SS** via transition state **TS4RR/RS/SR/SS**, the [1, 4]-proton transfer process to afford the zwitterionic intermediate **M5RR/RS/SR/SS** via transition state **TS5RR/RS/SR/SS**, the ring-closure process to form the five-membered heterocycle **M6RR/RS/SR/SS** via transition state **TS6RR/RS/SR/SS**, and the disassociation of the catalyst from the desired product **PRR/RS/SR/SS** via transition state **TS7RR/RS/SR/SS**. As presented in **Fig. 1** and **Fig. 2**, we have divided the free energy profiles into two parts including the free energy profiles of **Stages 1** (steps 1-3) and 2 (steps 4-7). In **Stage 1** (i.e. the activation stage, **Scheme 4**), the reaction proceeds under the NHC and Brønsted acid TMEDA·H^+ cooperative catalysis, and a TMEDA·H^+ molecule is included in the reaction models associated with the structural transformation from intermediate **M02$_B$** to intermediate **M06$_B$**, while the TMEDA·H^+ molecule is removed in the reaction models of **Stage 2** (i.e. the desorption stage). Because the significant difference between the models in the two stages, and the energy of the stationary point with TMEDA·H^+ (such as **Si-M06$_B$**) is much lower than that without TMEDA·H^+ (such as **Si-M3**), so we think it is not reasonable to connect the two energy profiles to each other directly. It should be noted that the subscript "D", "B", and "T" of the intermediates and transition states in **Stage 1** represent the direct proton transfer pathway, the TMEDA·H^+-assisted proton transfer pathway, and the TMEDA-assisted proton transfer pathway, respectively.

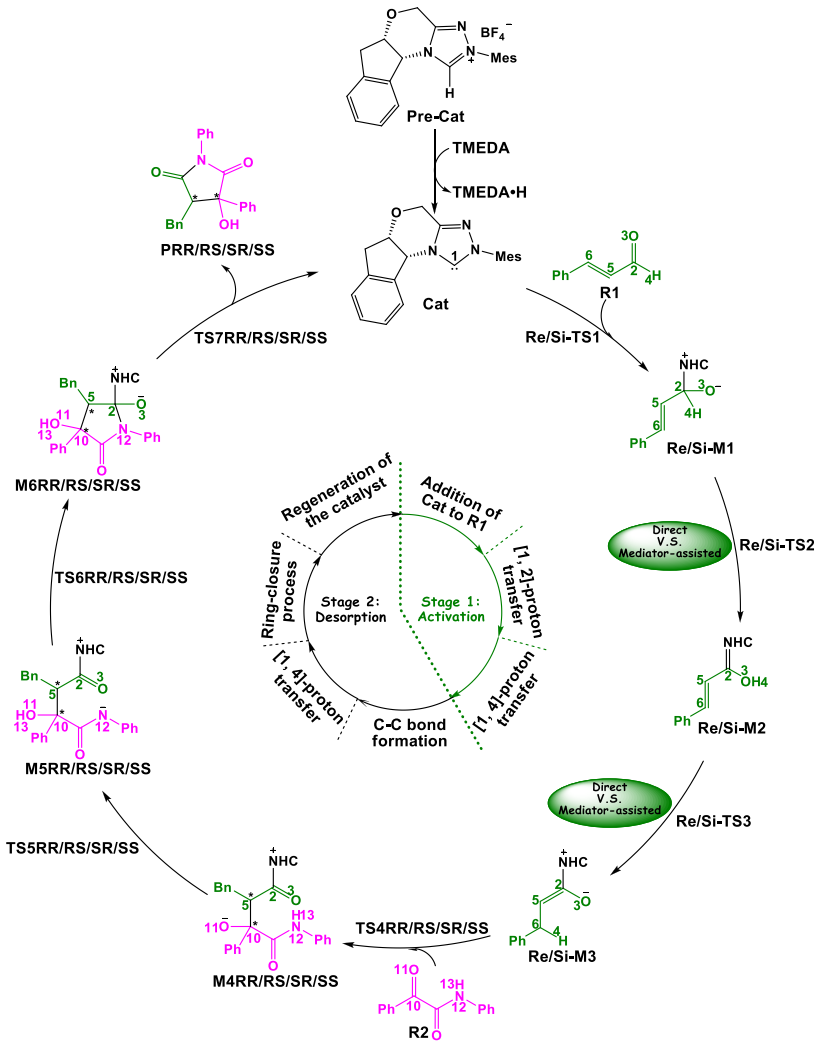

1

2 **Scheme 4** The entire catalytic cycle of the title reaction

3

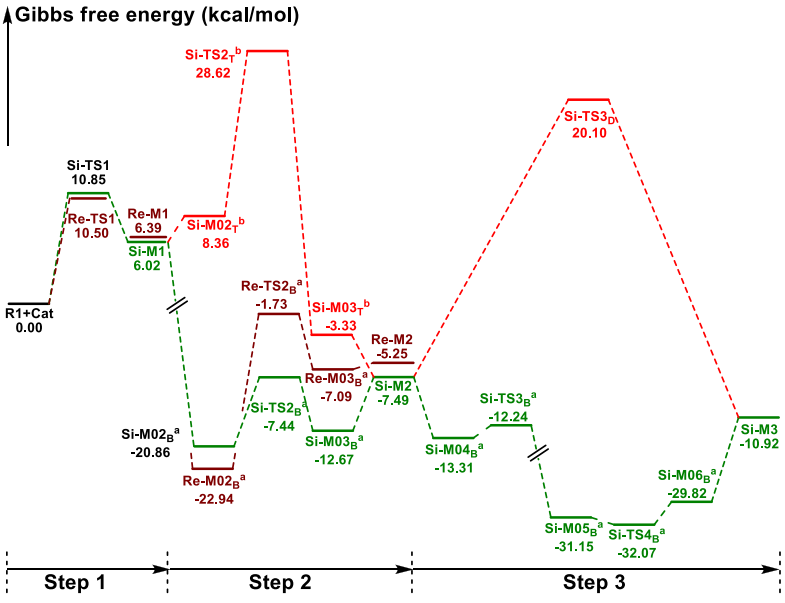

4

Fig. 1 The Gibbs free energy profiles of **Stage 1** of the title reaction. ([a] subtracting the free energy of TMEDA·H^+, [b] subtracting the free energy of TMEDA)

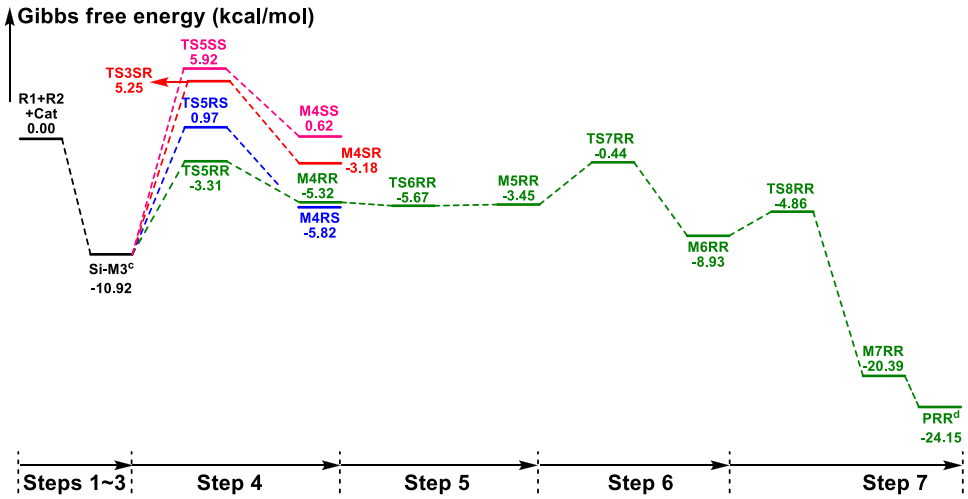

Fig. 2 The Gibbs free energy profiles of **Stage 2** involved in the title reaction. ([c] adding the free energy of **R2**, [d] adding the free energy of **Cat**)

First step: Nucleophilic addition of Cat to R1. As shown in **Scheme 4**, the precatalyst **4** would be deprotonated with the aid of base TMEDA to yield the actual catalyst **Cat** and *in situ* generates the Brønsted acid TMEDA·H^+.[15b, 22l] Then the zwitterionic intermediate **Re/Si-M1** is formed through the Re/Si-face nucleophilic attack on the C2 atom of **R1** by the C1 atom in **Cat** via the transition state **Re/Si-TS1**. The optimized structures and geometrical parameters depicted in **Fig. 3** show that the distance of C1–C2 is shortened from 2.00/2.04 Å in transition state **Re/Si-TS1** to 1.55/1.56 Å in the intermediate **Re/Si-M1**, which implies the complexation of the catalyst with the reactant. The Gibbs free energy barrier of this step (10.50/10.85 kcal/mol, **Fig. 1**) reveals that the reaction can occur smoothly under the experimental conditions. With regard to the stereoselectivity, as the free energy barrier difference via **Re-TS1** (10.50 kcal/mol, **Fig. 1**) in comparison to that via **Si-TS1** (10.85 kcal/mol, **Fig. 1**) is predicted to be a value that lies within the error bar of the computational method, it is difficult to determine whether **Re-M1** or **Si-M1** is preferred to be generated in the first step.

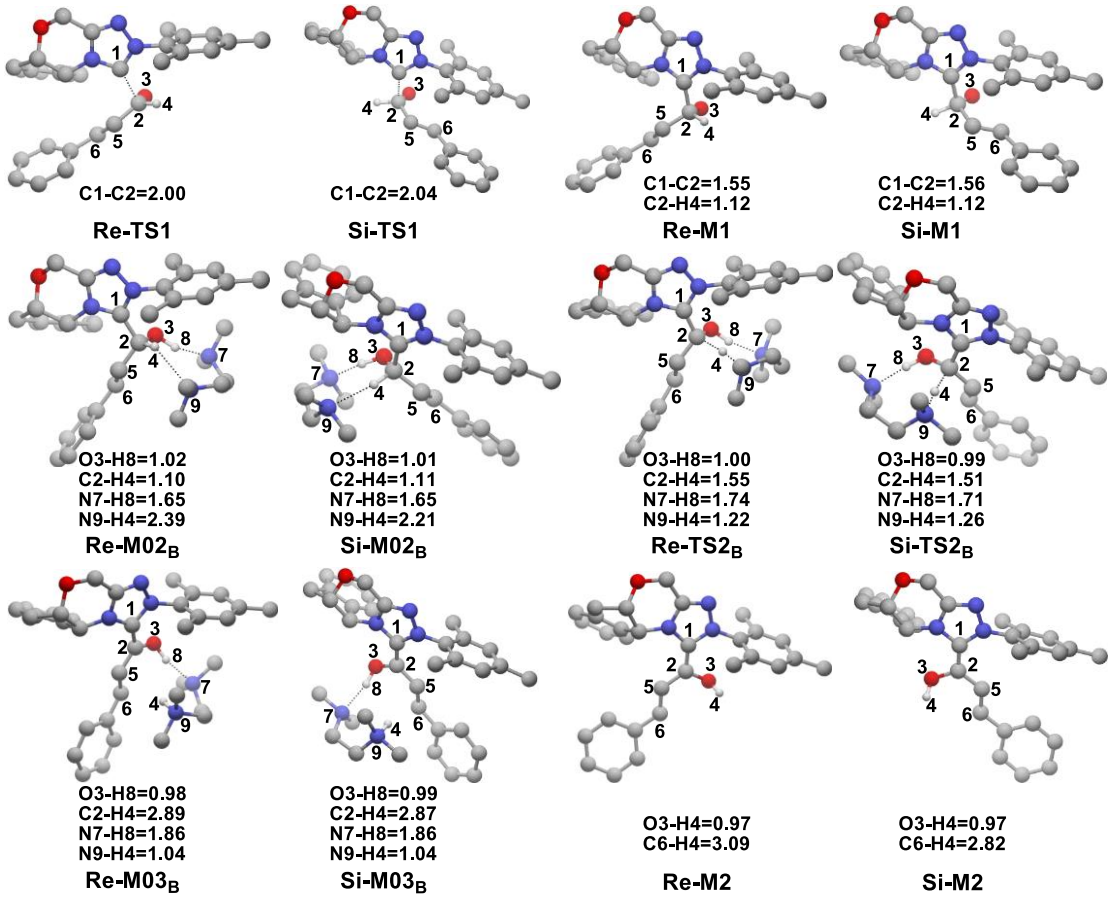

Fig. 3 The optimized structures and geometrical parameters involved in step 1 and step 2. (distance in Å and only the hydrogen involved in the reaction are shown for the sake of clarity)

Second Step: [1, 2]-proton transfer process. The second step is the [1, 2]-proton transfer process, in which the proton H4 transfers from C2 atom to O3 atom for the formation of Breslow intermediate. Many theoretical investigations show the direct [1, 2]-proton transfer mechanism is impossible to occur under a mild condition due to the large strain of the three-membered ring in transition state. As depicted in **Fig. 1**, our computational results[15] also confirm that the direct proton transfer process via transition state **Re/Si-TS2$_D$** encounters a significantly high energy barrier (50.03/44.31 kcal/mol, see ESI), indicating such a possibility is not likely under the mild condition.

It has been reported that the generation of the Breslow intermediate could be assisted by a base or protic media. In view of this, the previously formed Brønsted acid TMEDA·H$^+$ assisted proton transfer process has been taken into consideration. As depicted in **Scheme 5A**, the cleavage of C2–H bond and formation of hydroxyl O3–H bond are supposed to occur simultaneously in the

eight-membered ring transition state, however, the computational outcomes show that the elongated C2–H bond always reformed, the O3–H bond generated automatically, and the transition state turned into **Re/Si-M02$_B$** after optimization, which is due to the strong acidity of the Brønsted acid and basicity of the O3 atom. In other words, the O3 atom of **Re/Si-M1** is first protonated by Brønsted acid TMEDA·H$^+$ directly to give the intermediate **Re/Si-M02$_B$**. The O–H···N hydrogen bonds in intermediates **Re-M02$_B$** and **Si-M02$_B$** make them very stable with a free energy of –22.94/–20.86 kcal/mol (**Fig. 1**). The calculated results indicate that this step is a barrierless, highly exergonic, and irreversible process. Then the proton H4 located on C2 atom transfers to N9 atom of TMEDA via transition state **Re/Si-TS2$_B$** for the formation of intermediate **Re/Si-M03$_B$**. The distances of C2–H4 and N9–H4 are changed from 1.55/1.51 Å and 1.22/1.26 Å in transition state **Re/Si-TS2$_B$** to 2.89/1.04 Å and 2.87/1.04 Å in intermediate **Re/Si-M03$_B$** respectively, revealing the accomplishment of the proton transfer process and regeneration of the Brønsted acid TMEDA·H$^+$. After passing through a barrier of 21.21/13.42 kcal/mol (**Re/Si-TS2$_B$**, **Fig. 1**) and disassociation of Brønsted acid, the Breslow intermediate **Re/Si-M2** is formed completely. The calculated outcomes indicate that the reaction pathway for the formation of **Re-M2** ($\Delta G^{\neq}$=21.21 kcal/mol) is much less favorable than that leading to **Si-M2** ($\Delta G^{\neq}$=13.42 kcal/mol), therefore, we believe it is reasonable to omit the reaction pathway associated with the *Re* face attack on **R1** in the following parts.

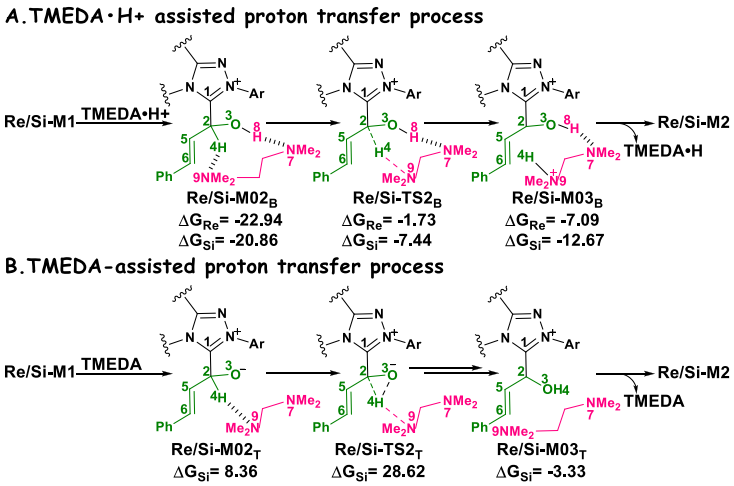

Scheme 5 The TMEDA·H$^+$- and TMEDA-assisted proton transfer pathways for the formation of Breslow intermediate (energies in kcal/mol).

In addition, we have also considered the base TMEDA-assisted proton transfer mechanism.

As shown in **Scheme 5B**, the reaction precursor **Si-M02$_T$** is first formed (we only calculated the *Si* addition pathway for sake of convenience), and then the N9 atom in TMEDA abstracts the proton H4 in C2 atom via transition state **Si-TS2$_T$**. The intermediate **Si-M03$_T$** is then formed by abstracting the H4 atom from N9 atom and this process is barrierless due to the strong basicity of the O3 atom. The energy barrier of this process is 28.62 kcal/mol, which is much higher than the TMEDA·H$^+$-assisted proton transfer process via transition state **Si-TS2$_B$** (13.42 kcal/mol, **Fig. 1**). Thus the TMEDA-assisted proton transfer mechanism is not favorable to occur under the experimental condition.

Taken together, two possible pathways for the proton transfer process to afford **Si-M2** have been suggested and studied. In this step, apart from the direct proton transfer mechanism, the *in situ* generated Brønsted acid TMEDA·H$^+$ mediated proton transfer mechanism for the formation of the Breslow intermediate **Si-M2** via transition state **Si-TS2$_B$** is energetically feasible than the other proton transfer processes.

Third Step: [1, 4]-proton transfer process to form the enolate intermediate. The subsequent reaction process is the [1, 4]-proton transfer for the formation of the enolate intermediate **Si-M3**, which includes two possible reaction pathways: the direct proton transfer process via a five-membered ring transition state and the Brønsted acid-assisted proton transfer process. As we have left out the reaction pathway associated with **Re-M2** in the second step, we only studied the reaction pathway associated with **Si-M2** in the following steps.

(1) Direct proton transfer process: For the direct proton transfer process, the H4 atom directly transfers from O3 atom to C6 atom for the formation of **Si-M3** via a five-membered transition state **Si-TS3$_D$**. The optimized structures and geometrical parameters depicted in **Fig. 4** show that the distance of O3–H4 is increased from 0.97 Å in intermediate **Si-M2** to 1.25 Å in transition state **TS3$_D$**, and finally to 2.54 Å in intermediate **Si-M3**, while that of C6–H4 is shortened from 1.44 Å in transition state **Si-TS3$_D$** to 1.10 Å in intermediate **Si-M3**, indicating that the proton transfer process is completed. Interestingly, the free energy barrier of this step is 27.59 kcal/mol with respect to **Si-M2** (**Fig. 1**), which is a little high for the formation of enolate intermediate **Si-M3** under the experimental conditions.

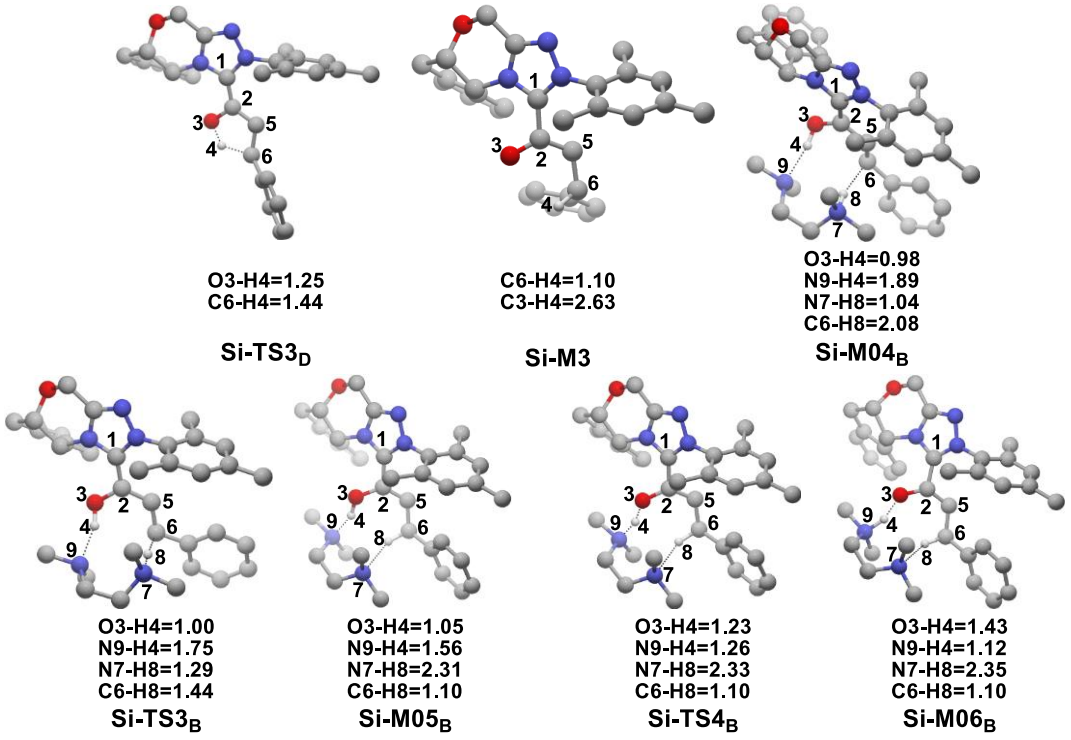

Fig. 4 The optimized structures and geometrical parameters involved in the third step. (distance in Å and only the hydrogen involved in the reaction are shown for the sake of clarity)

(2) Brønsted acid-assisted proton transfer process: As discussed above, the newly generated Brønsted acid can promote the proton transfer process in the second step. Thus, we also suggested and investigated the Brønsted acid-assisted proton transfer process in this step. It should be noted that we only can obtain the structures of the stepwise transition state when we tried to locate the concerted TMEDA•H^+ assisted [1, 4]-proton transfer transition state. As mapped in **Scheme 6**, the intermediate **Si-M2** and Brønsted acid TMEDA·H^+ first form a more stable complex **Si-M04$_B$** ($\Delta G^{\neq}$= –13.31 kcal/mol, **Fig. 1**) through electrostatic attraction between the two components and the formation of the O–H···N (the distance of H4–N9 is 1.89 Å, **Fig. 4**) and N–H···C hydrogen bonds (the distance of C6–H8 is 2.04 Å, **Fig. 4**). The TMEDA·H^+-assisted proton transfer process is calculated to be in a stepwise manner. Initially, the proton H8 transfers from N7 to C6 atoms via transition state **Si-TS3$_B$** to form intermediate **Si-M05$_B$** ($\Delta G^{\neq}$= –31.15 kcal/mol). Subsequently, the proton H4 smoothly transfers from O2 to N9 atom via transition state **Si-TS4$_B$** to give the enolate intermediate **Si-M3$_B$**.

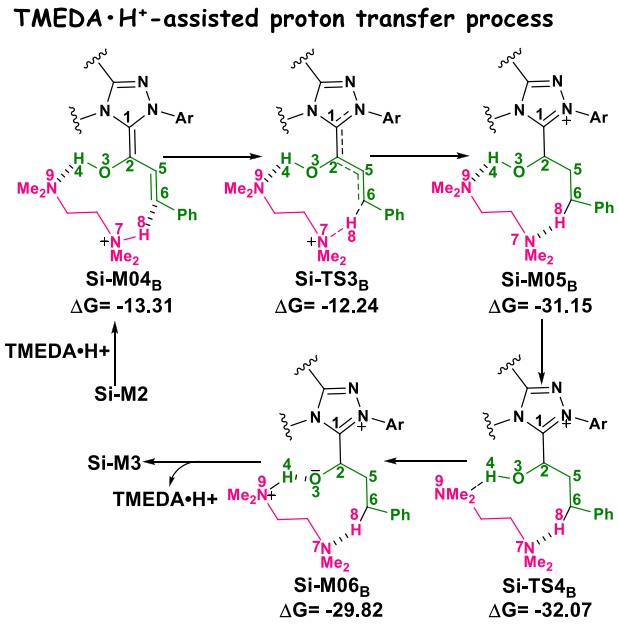

Scheme 6 The TMEDA·H$^+$-assisted proton transfer mechanism for the formation of enolate intermediate (energies in kcal/mol).

The free energy barrier calculated for the first process of the TMEDA·H$^+$-assisted proton transfer pathway is so low (1.07 kcal/mol via **Si-TS3$_B$**, **Fig. 1**), which indicates that it is easy to occur under the experimental conditions. The second process costs the free energy barrier of 0.92 kcal/mol based on the total energy (E, for details see ESI), but it is a barrierless process based on the free energy (G) profile depicted in **Fig. 1**. Overall, the free energy barrier of the TMEDA·H$^+$-assisted proton transfer mechanism is only 1.07 kcal/mol, and it is remarkably lower than that of the direct proton transfer pathway (**Si-TS3$_D$**).

In addition, as shown in **Scheme 4**, the enolate intermediate is necessary for the [2 + 3] cycloaddition, and we have further considered other two possible reaction pathway, i.e. the direct proton transfer from C2 to C6 atom and the TMEDA·H$^+$-assisted direct proton transfer from C2 to C6 atom, respectively. The calculated results show that the direct proton transfer pathway has an extremely high energy barrier (42.70 kcal/mol, **Scheme S1**), which is mainly due to the large strain of the four-membered ring in the transition state. It should be noted that only the structure of intermediate **Re/Si-M02$_B$** can be obtained when we put the structures of **Re/Si-M1** and TMEDA·H$^+$ together, that is to say, the proton can be transferred to O3 atom automatically, so we do not think the TMEDA·H$^+$-assisted direct proton transfer from C2 to C6 atom can occur.

Fourth Step: C–C bond formation process. As discussed above, the enolate intermediate **Si-M3** is formed in the third step and the subsequent step is the construction of C–C bond, which obviously needs to add a molecule of **R2**. By electrostatic attraction between C5 in intermediate **Si-M3** and C10 atoms in reactant **R2**, the C5–C10 single bond is formed in intermediate **M4** via transition state **TS5**. **Table 1** and **Scheme 7** illustrate the possible reaction patterns and the stereoselectivities for the C–C bond formation step involved in the fourth step. As summarized in **Table 1**, there are four possible reaction patterns, because the *Re* or *Si* face **of R2** can attack from either the *Re* or *Si* face of **Si-M3** in the reaction. As an important note, those different nucleophilic attack modes create the two chiral carbon centers, i.e., C5 and C10 atoms in the zwitterionic intermediate **M4RR/RS/SR/SS** via transition state **TS5RR/RS/SR/SS**. Since two contiguous chiral centers are formed in **M4RR/RS/SR/SS**, we term the first letter after **M4** as the chirality of C5 atom and the second letter as the chirality of C10 atom.

Table 1 Possible reaction patterns for the C-C bond formation step in fourth step

Addition face of **Si-M3**	Addition face of **R2**	Chirality of the C5 atom	Chirality of the C10 atom	Configuration of **M4**
Si	*Si*	R	R	RR
Si	*Re*	R	S	RS
Re	*Si*	S	R	SR
Re	*Re*	S	S	SS

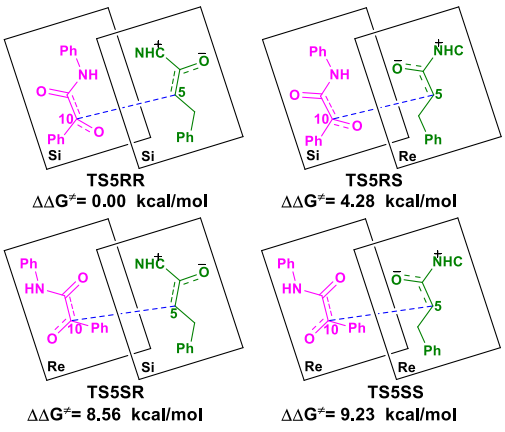

Scheme 7 Illustration of the stereochemistry.

With approaching of **R2** to **Si-M3**, the distance between C5 and C10 atoms changed from 1.99/2.04/2.08/2.03 Å in transition state **TS5RR/RS/SR/SS** to 1.64/1.60/1.57/1.65 Å in intermediate **M4RR/RS/SR/SS**, which implies that the full formation of the C5–C10 bond during the fourth step (**Fig. 7**). The free energy barriers of this step shown in **Fig. 2** are 7.61, 11.87, 16.17, and 16.84 kcal/mol with respect to **Si-M3**, respectively. Obviously, the formation of intermediate **M4RR** costs the lowest energy barrier and the energy barrier via **TS5RR** is 4.28~9.23 kcal/mol lower than those via **TS5RS/SR/SS**, which demonstrates that the formation **M4RR** is more energy favorable and supports the reported preference to form the product with RR-configuration. Thus, we think it is reasonable to only discuss the RR-configuration pathway as reference in the following parts. Furthermore, the energy barriers of this step in the NHC-catalyzed annulations with different substrates in DCM solvent have also been calculated, and the results summarized in **Table S3** of ESI show that the RR-configurational product is the main product, which are aligned well with the experimental observations and thus demonstrates our calculated results should be reliable.

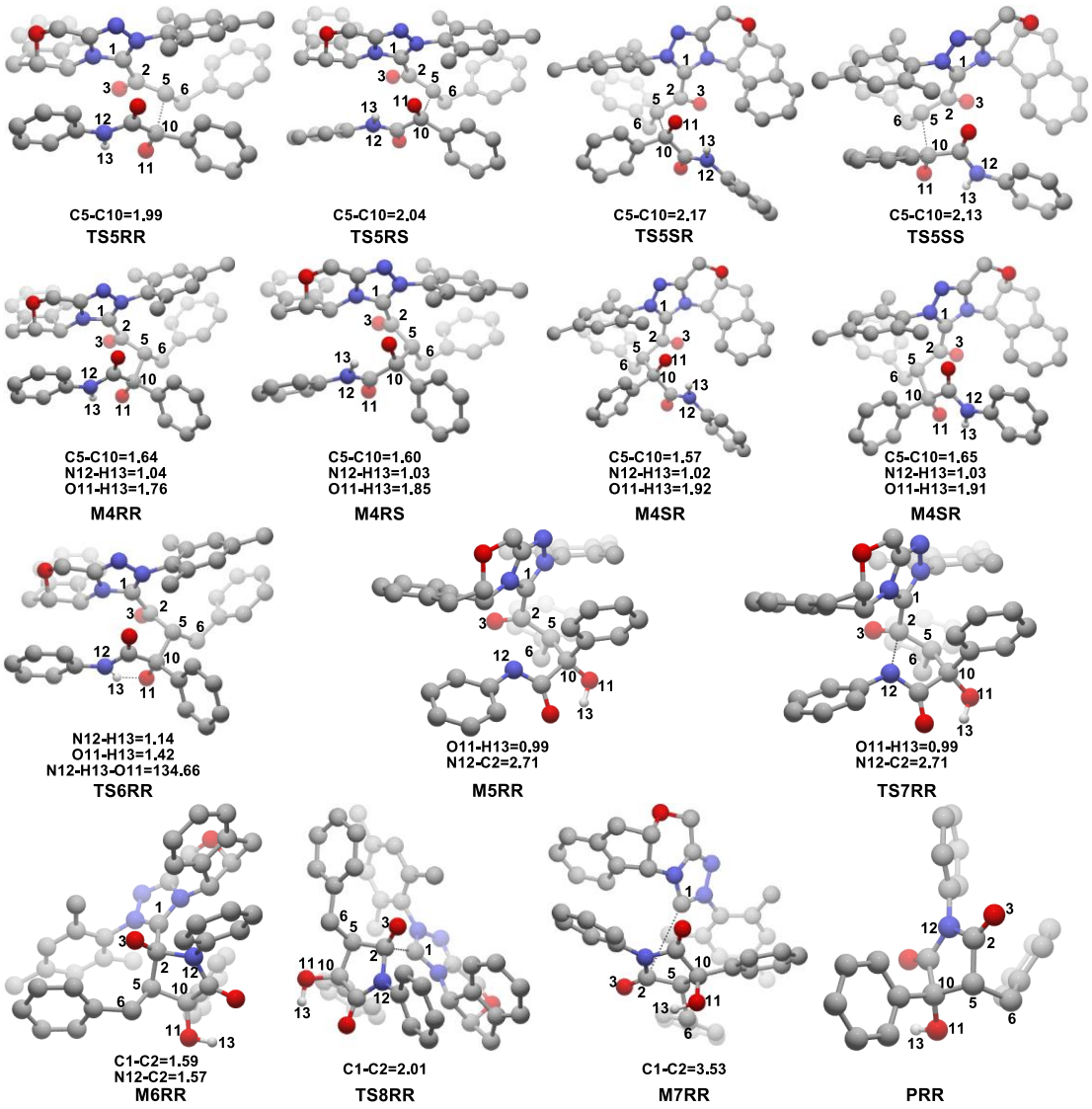

Fig. 5 The representative optimized structures and geometrical parameters involved in steps 5~7. (distance in Å and only the hydrogen involved in the reaction are shown for the sake of clarity)

Fifth Step: Intramolecular [1, 4]-proton transfer process. In this step, the formed intermediate **M4RR** transforms to the intermediate **M5RR** via [1, 4]-proton transfer process. The proton H13 transfers from N12 atom to O11 atom to form intermediate **M5RR** with the free energy of –3.45 kcal/mol (**Fig. 2**). It should be noted that the free energy of **M5RR** is higher than that of **TS6RR**, the reason could be that the strong hydrogen bond N–H···O in transition state **TS6RR** (O11–H13=1.42, N12–H13=1.14, O11–H13–N12=134.66°) and the missing of N–H···O hydrogen bond in intermediate **M5RR**, and the strain of the N12 and the carbonyl group to the right relative configuration for the following ring-colure process makes the relative energy of **M5RR** is a little higher than that of **TS6RR**. The energy barrier of this step is 3.34 kcal/mol based on the total

energy (*E*, see Supporting Information), while this step is calculated to be a barrierless process based on the free energy ($\Delta G^{\neq}$ = –0.08 kcal/mol, **Fig. 2**).

Sixth Step: The Ring-closure Step. As shown in **Scheme 4**, since intermediate **M5RR** is formed in the fifth step and the nucleophilic N12 atom orientates in a suitable trajectory that **R2** and enolate moieties overlap with each other in the maximal way. The following step is to construct the five-membered heterocycle, which is included in the final product. The negatively charged N12 atom nucleophilic attacks the C2 atom via transition state **TS7RR** for the formation of intermediate **M6RR**. The distance of C2–N12 is shortened from 2.71 Å in intermediate **M5RR** to 2.31 Å in transition state **TS7RR**, and finally to 1.57 Å in intermediate **M6RR**, demonstrating the full formation of C2–N12 bond. The energy profile mapped in **Fig. 2** shows that the formation of intermediate **M6RR** cost the energy barrier of 3.01 kcal/mol, showing that this step is a facile process and can occur smoothly under the experimental conditions.

Seventh Step: Regeneration of the Catalyst. The last step of this annulation reaction is the dissociation of the catalyst with the product via transition state **TS8RR**, and this leads to the regeneration of the catalyst. As shown in **Fig. 5**, the distance between C1 and C2 atoms is increased from 1.59 Å intermediate **M6RR** to 2.01 Å in transition state **TS8RR**, and finally to 3.53 Å in intermediate **M7RR**. The energy barrier of this step is only 4.07 kcal/mol, revealing that the dissociation process is a facilitated process and the catalyst is easy to regenerate. Finally, the desired product is formed by separating of the catalyst and product.

3.2 Origin of the Stereoselectivity

For the organocatalytic reaction, it is important to figure out the factors governing the stereoselectivities within the established mechanism. As discussed above, the entire reaction mechanisms contain more than one step, and the most energy favorable reaction mechanism for the entire energy profile of the NHC-catalyzed [3 + 2] annulation reaction is the *Si* face addition of **R1** to **Cat**, and the Brønsted acid-assisted proton transfer mechanism are the most favorable pathway. Starting from intermediate **Si-M3**, the two chirality centers (C5 and C10 atoms) are emerged in the C–C bond formation step, so we think that the transition states **TS5RR/RS/SR/SS** involved in this step is crucial for the stereoselectivity. As shown in **Fig. 2** and **Scheme 7**, the computed energy difference between the transition states **TS5RR** and **TS5SS** is 9.23 kcal/mol, and

the energy difference between the diastereomeric **TS5RR** and **TS5RS** is 4.28 kcal/mol, which corresponds to an enantiomeric excess of >99% in favor of the RR diastereomer. These predictions are in good accordance with the experimentally observed *ee* of 99%. To obtain deep insights into the origins of the stereoselectivity for the NHC-catalyzed [3 + 2] annulation reaction, we then performed the distortion/interaction analysis of the transition states **TS5**. The distortion/interaction analysis[30] is a fragment approach to understand organic reactions, in which the height of the energetic barrier is described in terms of the original reactants. As depicted in **Fig. 6**, the activation energy of the transition state is decomposed into to two main components: the distortion ($\Delta E_{dist}^{\neq}$) and the interaction ($\Delta E_{int}^{\neq}$) energy. The distortion energy involves geometric and electronic changes to deform the reactants into their transition state geometry, which involves bond stretching, angle decrease or increase, dihedral changes and so on. The interaction energy contains repulsive exchange-repulsive and stabilizing electrostatic, polarization, and orbital effects in the transition state structure. The interaction energy is recovered by the relationship: $\Delta E_{int}^{\neq} = \Delta E^{\neq} - \Delta E_{dist}^{\neq}$.

The calculated distortion and interaction energies of the reactants in transition state geometries are listed in **Table 2**. Comparing with the distortion/interaction energies of these four transition states, the distortion energies of **TS5RR** (28.32 kcal/mol, **Table 2**) is larger than those of **TS5RS** and **TS5SR** (23.11 and 22.32 kcal/mol, **Table 2**), but the larger distortion energies of **TS5RR** is offset by the largest interaction energy discrepancy (–39.80 kcal/mol, **Table 2**), and this is the dominant factor determining the RR-configuration product generated preferentially.

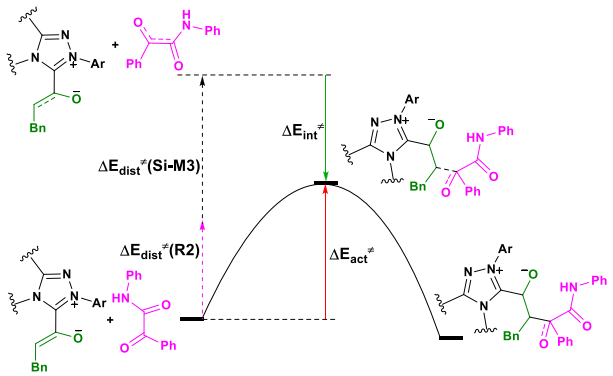

Fig. 6 The relationship between the activation energy, distortion and interaction energies of reaction patterns.

Table 2 The distortion/interaction reactivity analysis for the stereoselectivity-determining step of

the title reaction (All values are in kcal/mol).

	$\Delta\Delta G^{\neq}$	$\Delta E^{\neq}_{dist}$		$\Delta E^{\neq}_{act}$	$\Delta E^{\neq}_{int}$
		$\Delta E^{\neq}_{dist}$(**Si-M5**)	$\Delta E^{\neq}_{dist}$(**R2**)		
TS5RR	0	11.36	14.96	−13.48	−39.80
TS5RS	4.28	8.64	14.47	−9.68	−32.79
TS5SR	8.56	8.90	13.42	−1.64	−23.96
TS5SS	9.23	11.99	16.73	−3.73	−32.45

Note: (a) The $\Delta E^{\neq}$ value is the calculated total energy (E) of each transition state relative to the sum of the total energies of the two separate reactants.

As discussed above, the distortion/interaction analysis reveals the existence of interactions between enolate (**Si-M3**) and α-ketoamide (**R2**) moieties. To further identify the type of these interactions, we have then performed the non-covalent interaction (NCI) analysis, which is demonstrated to be capable of distinguishing strong interaction, van der Waals interactions and repulsive steric interactions. **Figs. 7** and **S4** show the NCI results for the transition states **TS5RR**, **TS5RS**, **TS5SR**, and **TS5SS**. In **TS5RR**, there are three CH···π interactions, one π···π interaction, and one LP-π interaction. Specifically, the distances between the inner hydrogen and phenyl group are 2.39 Å (CH-π interaction a, **Fig. 7**), 2.62 Å (CH-π interaction b, **Fig. 7**), and 2.87 Å (CH-π interaction c, **Fig. 7**) separately, well within the combined van der Waals distance of 2.90 Å. As can be seen from **Fig. S4** of ESI, the CH-π and π-π interactions can also be observed in the other transition states between the π-system of enolate and **R2** moieties. Noteworthy, the noncovalent interactions indeed seem to be not significantly different among the four NCI pictures.

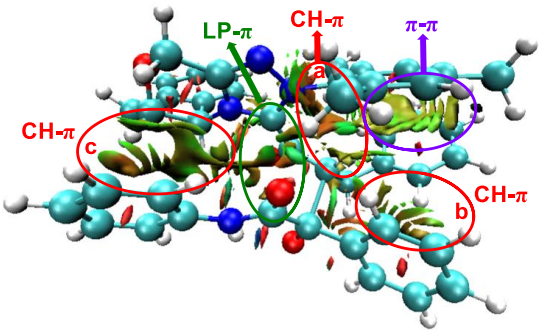

Fig. 7 The interaction analysis of the transition state **TS5RR**. (Blue, green, and red represent the strong interaction, weak interaction, and steric effect, respectively)

Furthermore, the natural bond orbital (NBO) analysis of the reaction active site is performed to explain the origin of the stereoselectivity. As shown in **Fig. S5** of ESI, the net NBO charge values on the C2=C5 π system are 0.060 *e* (**TS5RR**), 0.049 *e* (**TS5RS**), 0.028 *e* (**TS5SR**), and 0.015 *e* (**TS5SS**), respectively. Obviously, the NBO charge populated on C2=C5 π system is more positive in **TS5RR** than that in the other three transition states, this phenomenon indicates that the more electron delocalization in **TS5RR** stabilizes the transition state and makes the RR-configuration isomer prominent. Then, we have performed frontier molecular orbital analysis for the stereoselectivity-determining step, which mainly involves the orbital interaction between $HOMO_{Si\text{-}M3}$ and $LUMO_{R2}$. As shown in **Fig. 8**, the energy gaps between $HOMO_{M3\text{-}part}$ and $LUMO_{R2\text{-}part}$ are 3.68, 3.79, 3.93, and 4.02 eV in the four key transition states **TS5RR**, **TS5RS**, **TS5SR**, and **TS5SS** respectively, indicating the energy gap in transition state **TS5RR** is narrowest, thus, the reaction pathway associated with transition state **TS5RR** should have the lowest energy barrier and be the most favorable pathway, which is in agreement with the above energy profiles and experimental results.

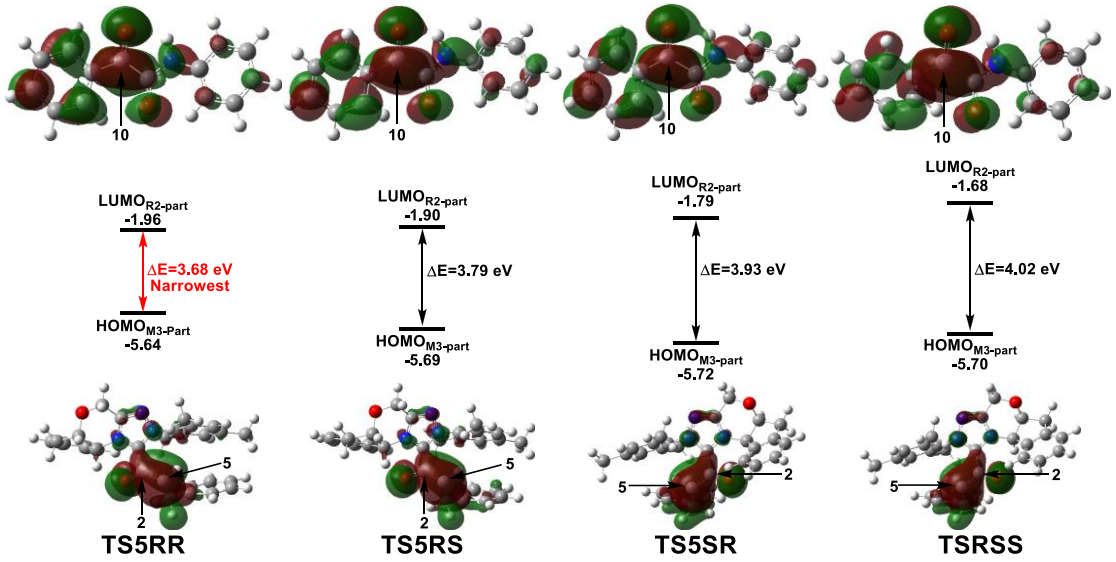

Fig. 8 The energy gaps between $HOMO_{M3\text{-}part}$ and $LUMO_{R2\text{-}part}$ parts in the four transition states **TS5RR**, **TS5RS**, **TS5SR**, and **TS5SS**.

3.3 Role of the NHC Catalyst

Having established the most favorable reaction pathway and the origin of the stereoselectivity,

we now explore the special role of the NHC catalyst in this [3 + 2] annulation reaction. The natural bond orbital (NBO) charge value of H4 atom is slightly increased from 0.168 e in the enal (**R1**) to 0.178 e in intermediate **Si-M1**, which indicates that the NHC strengthens the acidity of the H4 atom, this would make the breaking of C−H bond more easily. This phenomenon shows that the NHC catalyst can activate the carbonyl C−H bonds of enals by strengthening acidity of the H4 atom.

In addition, our previous work[18] has proved that the NHC catalyst plays as a role of Lewis base by the analysis of global reactivity indexes (GRI) in the NHC catalyzed ketene cycloadditions. Thus, we also want to know if the NHC plays the same role in this reaction system. With this question promotion, the analysis of GRI was performed in this work. As summarized in **Table 3**, the molecule global electrophilicity character is measured by electrophilicity index, ω, which has been given from the following expression, $\omega = (\mu^2/2\eta)$,[31] in terms of the electronic chemical potential μ and the chemical hardness η. Both quantities may be approached in terms of the one-electron energies of the frontier molecular orbital HOMO and LUMO, E_H and E_L, as $\mu \approx (E_H + E_L)/2$ and $\eta \approx (E_L - E_H)$. Moreover, according the HOMO energies obtained within the Kohn-Sham scheme,[32] Domingo and co-workers gave the nucleophilicity index N to handle a nucleophilicity scale.[33] The nucleophilicity index is defined as $N = E_{H(SR)} - E_{H(TCE)}$. This nucleophilicity scale is referred to tetracyanoethylene (TCE) taken as reference. After the coordination with NHC catalyst, the electrophilicity of enal is dramatically decreased, but its nucleophilicity is increased greatly from 2.504 to 3.498/3.514 eV (**Re/Si-M1**), and finally to 4.302 eV (**Si-M3**). Thus, the GRI analysis demonstrates that the NHC catalyst mainly works as Lewis base catalyst to strengthen the nucleophilicity of the reactant enal.

Table 3 Energies of HOMO (E_L, a.u.) and LUMO (E_L, a. u.), Electronic Chemical Potential (μ, a.u.), Chemical Hardness (η, eV), Global Electrophilicity (ω,eV), and Global Nucleophilicity (N, eV) of Some Reactants (SR)

SR	E_H (a.u.)	E_L (a.u.)	μ (a.u.)	η (a.u.)	ω (eV)	N^a (eV)
R1	−0.28623	−0.04411	−0.16517	0.24212	1.533	2.504
Re-M1	−0.24973	0.00474	−0.122495	0.25447	1.605	3.498
Si-M1	−0.24912	−0.00203	−0.125575	0.24709	1.737	3.514
Si-M3	−0.22018	−0.00374	−0.11196	0.21644	1.576	4.302

[a] $E_{H(TCE)}$= −0.37826 a.u. (calculated at M06-2X/6-31G**/IEF-PCM$_{DCM}$ level).

In summary, the results of NBO and GRI analysis reveal that the NHC plays as a bifunctional organocatalyst in this novel [3 + 2] annulation reaction of enals. That is to say, the NHC catalyst not only works as the Lewis base catalyst to strengthen the nucleophilicity of the enals, but also activates the carbonyl C-H bonds in the subsequent proton transfer processes.

4. Conclusion

In this article, the comprehensive DFT calculations on the NHC-catalyzed intermolecular [3 + 2] annulation reaction of enals with α-ketoamides have been performed to pursuit deep understanding of the detailed mechanisms and stereoselectivity. On the basis of our calculations, the most energy favorable reaction mechanism is demonstrated to occur through seven elementary steps, i.e., addition of the catalyst, formation of Breslow intermediate, formation of enolate intermediate, C−C bond formation step, proton transfer process, ring-closure process and the regeneration of the catalyst. The calculated results reveal that the *in situ* generated Brønsted acid TMEDA·H^+ plays an important role in the [1, 2]- and [1, 4]-proton transfer processes associated with the formation of Breslow intermediate and enolate intermediate, respectively. The C–C bond formation step are verified to be the stereoselectivity-determining step, and the two chiral centers (C5 and C10 atoms) are determined by the *Re* or *Si* face addition of **R2** with the *Re* or *Si* face of **Si-M3**. The strong interaction and electron delocalization of the reaction active site was demonstrated to be responsible for the favorability of RR-configured product by the distortion/interaction, NCI, and NBO analyses. All the calculated results are in good agreement with the experimental observations.

Furthermore, the analyses of NBO and GRI were carried out to explore the role of the NHC catalyst in this kind of reactions. The computational outcomes reveal that the NHC catalyst works as a bifunctional organocatalyst, i.e. Lewis base and the carbonyl C-H activation. The new insights gained from this work might help to refine the stereochemistry model of NHC-catalyzed [3 + 2] cycloaddition reactions and be beneficial for the future development of this field as well as design of novel efficient catalyst.

ACKNOWLEDGMENTS

The work described in this paper was supported by the National Natural Science Foundation of China (no. 21303167), China Postdoctoral Science Foundation (nos. 2013M530340 and 2015T80776) and Excellent Doctoral Dissertation Engagement Fund of Zhengzhou University in 2014.

REFERENCES

1. (a) D. M. Flanigan, F. Romanov-Michailidis, N. A. White and T. Rovis, *Chem. Rev.*, 2015, **115**, 9307; (b) D. Enders, O. Niemeier and A. Henseler, *Chem. Rev.*, 2007, **107**, 5606; (c) F. Glorius and K. Hirano, *Springer-Verlag: Berlin, Heidelberg*, 2008, **2**, 159; (d) J. L. Moore and T. Rovis, *Top. Curr. Chem.*, 2010, **291**, 77; (e) D. Enders and T. Balensiefer, *Acc. Chem. Res.*, 2004, **37**, 534; (f) V. Nair, S. Vellalath and B. P. Babu, *Chem. Soc. Rev.*, 2008, **37**, 2691; (g) M. Fèvre, J. Pinaud, Y. Gnanou, J. Vignolle and D. Taton, *Chem. Soc. Rev.*, 2013, **42**, 2142.

2. (a) J. Xu, C. Mou, T. Zhu, B. A. Song and Y. R. Chi, *Org. Lett.*, 2014, **16**, 3272; (b) M. Wang, Z. J. Huang, J. F. Xu and Y. R. Chi, *J. Am. Chem. Soc.*, 2014, **136**, 1214; (c) H. M. Zhang, Z. H. Gao and S. Ye, *Org. Lett.*, 2014, **16**, 3079; (d) Y. Zhang, Y. Y. Lu, W. F. Tang, T. Lu and D. Du, *Org. Biomol. Chem.*, 2014, **12**, 3009; (e) S. H. Hu, B. Y. Wang, Y. Zhang, W. F. Tang, M. Y. Fang, T. Lu and D. Du, *Org. Biomol. Chem.*, 2015, **13**, 4661; (f) A. Lee and K. A. Scheidt, *Chem. Commun.*, 2015, **51**, 3407; (g) Z. Q. Liang, Z. H. Guo, W. Q. Jia and S. Ye, *Chem. Eur. J.*, 2015, **21**, 1868; (h) H. Lu, J. Y. Liu, C. G. Li, J. B. Lin, Y. M. Liang and P. F. Xu, *Chem. Commun.*, 2015, **51**, 4473; (i) X. Q. Fang, X. K. Chen and Y. R. Chi, *Org. Lett.*, 2011, **13**, 4708; (j) T. Wang, X. L. Huang and S. Ye, *Org. Biomol. Chem.*, 2010, **8**, 5007; (k) D. E. A. Raup, B. Cardinal-David, D. Holte and K. A. Scheidt, *Nat. Chem.*, 2010, **2**, 766; (l) J. Kaeobamrung, M. C. Kozlowski and J. W. Bode, *Proc. Natl. Acad. Sci. U. S. A.*, 2010, **107**, 20661; (m) X. K. Chen, X. Q. Fang and Y. R. Chi, *Chem. Sci.*, 2013, **4**, 2613; (n) L.-H. Sun, Z.-Q. Liang, W.-Q. Jia and S. Ye, *Angew. Chem. Int. Ed.*, 2013, **52**, 5803.

3. (a) X. L. Huang, X. Y. Chen and S. Ye, *J. Org. Chem.*, 2009, **74**, 7585; (b) X. N. Wang, P. L. Shao, H. Lv and S. Ye, *Org. Lett.*, 2009, **11**, 4029; (c) X. N. Wang, L. T. Shen and S. Ye, *Org. Lett.*, 2011, **13**, 6382.

4. X. N. Wang, L. T. Shen and S. Ye, *Chem. Commun.*, 2011, **47**, 8388.

5. (a) T. Y. Jian, X. Y. Chen, L. H. Sun and S. Ye, *Org. Biomol. Chem.*, 2013, **11**, 158; (b) T. Y. Jian, P. L. Shao and S. Ye, *Chem. Commun.*, 2011, **47**, 2381.

6. (a) C. Burstein and F. Glorius, *Angew. Chem. Int. Ed.*, 2004, **43**, 6205; (b) S. S. Sohn, E. L. Rosen and J. W. Bode, *J. Am. Chem. Soc.*, 2004, **126**, 14370; (c) H. Lv, B. Tiwari, J. M. Mo, C. Xing and Y. R. Chi, *Org. Lett.*, 2012, **14**, 5412; (d) H. Lv, W. Q. Jia, L. H. Sun and S. Ye, *Angew. Chem. Int. Ed.*, 2013, **125**, 8769; (e) C. Guo, M. Schedler, C. G. Daniliuc and F. Glorius, *Angew. Chem. Int. Ed.*, 2014, **53**, 10232; (f) A. Chan and K. A. Scheidt, *J. Am. Chem. Soc.*, 2007, **129**, 5334; (g) E. M. Phillips, T. E. Reynolds and K. A. Scheidt, *J. Am. Chem. Soc.*, 2008, **130**, 2416; (h) T. Zhu, P. Zheng, C. Mou, S. Yang, B. A. Song and Y. R. Chi, *Nat. Commun.*, 2014, **5**, 5027; (i) Z. Q. Liang, Z. H. Gao, W. Q. Jia and S. Ye, *Chem. Eur. J.*, 2015, **21**, 1868; (j) M. Wang, Z. Q. Rong and Y. Zhao, *Chem. Commun,*, 2014, **50**, 15309.

7. (a) Y. Q. Lin, L. M. Yang, Y. Deng and G. F. Zhong, *Chem. Commun.*, 2015, **51**, 8330; (b) Z. Q. Fu, H.

Sun, S. J. Chen, B. Tiwari, G. H. Li and Y. R. Chi, *Chem. Commun.*, 2013, **49**, 261.

8. (a) X. Y. Chen, F. Xia, J. T. Cheng and S. Ye, *Angew. Chem. Int. Ed.*, 2013, **52**, 10644; (b) J. M. Mo, X. K. Chen and Y. R. Chi, *J. Am. Chem. Soc.*, 2012, **134**, 8810; (c) R. Liu, C. X. Yu, Z. X. Xiao, T. J. Li, X. S. Wang, Y. W. Xie and C. S. Yao, *Org. Biomol. Chem.*, 2014, **12**, 1885.

9. (a) L. H. Sun, Z. Q. Liang, W. Q. Jia and S. Ye, *Angew. Chem. Int. Ed.*, 2013, **52**, 5803; (b) X. Fang, X. Chen, H. Lv and Y. R. Chi, *Angew. Chem. Int. Ed.*, 2011, **50**, 11782; (c) D. A. DiRocco and T. Rovis, *J. Am. Chem. Soc.*, 2011, **133**, 10402.

10. L. M. Fang, F. Wang, P. J. Chua, Y. B. Lv, L. J. Zhong and G. F. Zhong, *Org. Lett.*, 2012, **14**, 2894.

11. (a) S. R. Yetra, S. Mondal, E. Suresh and A. T. Biju, *Org. Lett.*, 2015, **17**, 1417; (b) J. D. Tessier, E. A. O'Bryan, T. B. H. Schroeder, D. T. Cohen and K. A. Scheidt, *Angew. Chem. Int. Ed.*, 2012, **124**, 5047; (c) A. G. Kravina, J. Mahatthananchai and J. W. Bode, *Angew. Chem. Int. Ed.*, 2012, **51**, 9433.

12. (a) J. Izquierdo, A. Orue and K. A. Scheidt, *J. Am. Chem. Soc.*, 2013, **135**, 10634; (b) Y. W. Xie, Y. L. Que, T. J. Li, L. Zhu, C. X. Yu and C. S. Yao, *Org. Biomol. Chem.*, 2015, **13**, 1829.

13. L. Wang, Q. Ni, M. Blumel, T. Shu, G. Raabe and D. Enders, *Chem. Eur. J.*, 2015, **21**, 8033.

14. S. E. Allen, J. Mahatthananachai, J. W. Bode and M. C. Kozlowski, *J. Am. Chem. Soc.*, 2012, **134**, 12098.

15. (a) Z. Y. Li, D. H. Wei, Y. Wang, Y. Y. Zhu and M. S. Tang, *J. Org. Chem.*, 2014, **79**, 3069; (b) Y. Wang, L. J. Zheng, D. H. Wei and M. S. Tang, *Org. Chem. Front.*, 2015, **2**, 874.

16. (a) P. Verma, P. A. Patni and R. B. Sunoj, *J. Org. Chem.*, 2011, **76**, 5606; (b) Y. Reddi and R. B. Sunoj, *Org. Lett.*, 2012, **14**, 2810; (c) R. Kuniyil and R. B. Sunoj, *Org. Lett.*, 2013, **15**, 5040.

17. Y. Qiao, D. Wei and J. Chang, *J. Org. Chem.*, 2015, **80**, 8619.

18. (a) M. M. Zhang, D. H. Wei, Y. Wang, S. J. Li, J. F. Liu, Y. Y. Zhu and M. S. Tang, *Org. Biomol. Chem.*, 2014, **12**, 6374; (b) D. H. Wei, Y. Y. Zhu, C. Zhang, D. Z. Sun, W. J. Zhang and M. S. Tang, *J. Mol. Catal. A: Chem.*, 2011, **334**, 108.

19. W. J. Zhang, D. H. Wei and M. S. Tang, *J. Org. Chem.*, 2013, **78**, 11849.

20 W. J. Zhang, Y. Y. Zhu, D. H. Wei, Y. X. Li and M. S. Tang, *J. Org. Chem.*, 2012, **77**, 10729.

21. M. J. Frisch, G. W. Trucks, H. B. Schlegel, G. E. Scuseria, M. A. Robb, J. R. Cheeseman, G. Scalmani, V. Barone, B. Mennucci, G. A. Petersson, H. Nakatsuji, M. Caricato, X. Li, H. P. Hratchian, A. F. Izmaylov, J. Bloino, G. Zheng, J. L. Sonnenberg, M. Hada, M. Ehara, K. Toyota, R. Fukuda,, M. I. J. Hasegawa, T. Nakajima, Y. Honda, O. Kitao, H. Nakai, T. Vreven, J. A. Montgomery Jr., J. E. Peralta, F. Ogliaro, M. Bearpark, J. J. Heyd, E. Brothers, K. N. Kudin, V. N. Staroverov, R. Kobayashi, J. Normand, K. Raghavachari, A. Rendell, J. C. Burant, S. S. Iyengar, J. Tomasi, M. Cossi, N. Rega, J. M. Millam, M. Klene, J. E. Knox, J. B. Cross, V. Bakken, C. Adamo, J. Jaramillo, R. Gomperts, R. E. Stratmann, O. Yazyev, A. J. Austin, R. Cammi, C. Pomelli, J. W. Ochterski, R. L. Martin, K. Morokuma, V. G. Zakrzewski, G. A. Voth, P. Salvador, J. J. Dannenberg, S. Dapprich, A. D. Daniels, Ö. Farkas, J. B. Foresman, J. V. Ortiz, J. Cioslowski and D. J. Fox, *GAUSSIAN 09* (*Revision C.01*), Gaussian, Inc., Wallingford, CT, 2010.

22. (a) Y. Qiao and K. L. Han, *Org. Biomol. Chem.*, 2012, **10**, 7689; (b) D. H. Wei, B. L. Lei, M. S. Tang and C. G. Zhan, *J. Am. Chem. Soc.*, 2012, **134**, 10436; (c) L. Zhang and D. C. Fang, *J. Org. Chem.*, 2013, **78**, 2405; (d) Y. M. Chen, G. A. Chass and D. C. Fang, *Phys. Chem. Chem. Phys.*, 2014, **16**, 1078; (e) Y. Li and D. C. Fang, *Phys. Chem. Chem. Phys.*, 2014, **16**, 15224; (f) Y. Li and Z. Y. Lin, *Org. Chem. Front.*, 2014, **1**, 1188; (g) Y. Wang, D. H. Wei, Z. Y. Li, Y. Y. Zhu and M. S. Tang, *J. Phys. Chem. A*, 2014, **118**, 4288; (h) A. N. Hancock, Y. Kavanagh and C. H. Schiesser, *Org. Chem. Front.*, 2014, **1**, 645; (i) Y. Wang, D. H. Wei, W. J. Zhang, Y. Y. Wang, Y. Y. Zhu, Y. Jia and M. S. Tang, *Org. Biomol. Chem.*,

2014, **12**, 7503; (j) D. Leboeuf, M. Gaydou, Y. H. Wang and A. M. Echavarren, *Org. Chem. Front.*, 2014, **1**, 759; (k) M. Quan, G. Q. Yang, F. Xie, L. Gridney and W. Zhang, *Org. Chem. Front.*, 2015, **2**, 398; (l) Q. Zhang, H. Z. Yu and Y. Fu, *Org. Chem. Front.*, 2014, **1**, 614; (m) D. M. Li, Y. Wang and K. L. Han, *Coord. Chem. Rev.*, 2012, **256**, 1137; (n) Y. Wang, X. Guo, M. Tang and D. Wei, *J. Phys. Chem. A*, 2015, **119**, 8422. (o) S. S. Chen, Y. Su, K. L. Han and X. W. Li, Org. Chem. Front., 2015, **2**, 783-791. (p) X. K. Guo, L. B. Zhang, D. H. Wei and J. L. Niu, Chem. Sci., 2015, **6**, 7059-7071.

23. (a) Y. Zhao and D. G. Truhlar, *Theor. Chem. Acc.*, 2008, **120**, 215; (b) Y. Zhao and D. G. Truhlar, *Acc. Chem. Res.*, 2008, **41**, 157.

24. (a) B. Mennucci and J. Tomasi, *J. Chem. Phys.*, 1997, **106**, 5151; (b) V. Barone and M. Cossi, *J. Phys. Chem. A*, 1998, **102**, 1995.

25. (a) C. Gonzalez and H. B. Schlegel, *J. Chem. Phys.*, 1989, **90**, 2154; (b) C. Gonzalez and H. B. Schlegel, *J. Phys. Chem.*, 1990, **94**, 5523.

26. (a) J. P. Foster and F. Weinhold, *J. Am. Chem. Soc.*, 1980, **102**, 7211; (b) A. E. Reed and F. Weinhold, *J. Chem. Phys.*, 1983, **78**, 4066; (c) E. D. Glendening, A. E. Reed, J. E. Carpenter and F. Weinhold, *NBO Version 3.1*.

27. T. Lu and F. W. Chen, *J. Comp. Chem.*, 2012, **33**, 580.

28. C. Y. Legault, *CYLview, 1.0b; Université de Sherbrooke, 2009 (http://www.cylview.org)*.

29. J. D. Chai and M. H. Gordon, *Phys. Chem. Chem. Phys.*, 2008, **10**, 6615.

30. (a) R. Gordillo and K. N. Houk, *J. Am. Chem. Soc.*, 2006, **128**, 3543; (b) C. D. Anderson, T. Dudding, R. Gordillo and K. N. Houk, *Org. Lett.*, 2008, **10**, 2749; (c) O. Gutierrez, R. G. Iafe and K. N. Houk, *Org. Lett.*, 2009, **11**, 4298; (d) M. A. M. Capozzi, C. Centrone, G. Fracchiolla, F. Naso and C. Cardellicchio, *Eur. J. Org. Chem.*, 2011, 4327.

31. (a) R. G. Parr and R. G. Pearson, *J. Am. Chem. Soc.*, 1983, **105**, 7512; (b) L. R. Domingo, M. T. Picher and J. A. Saez, *J. Org. Chem.*, 2009, **74**, 2726.

32. (a) L. J. Sham and W. Kohn, *Phys. Rev.*, 1966, **145**, 561; (b) W. Kohn and L. J. Sham, *Phys. Rev.*, 1965, **137**, 1697.

33. (a) L. R. Domingo, E. Chamorro and P. Perez, *J. Phys. Chem. A*, 2008, **112**, 4046; (b) L. R. Domingo, E. Chamorro and P. Perez, *J. Org. Chem.*, 2009, **2009**, 3036; (c) L. R. Domingo, P. Perez and J. A. Saez, *RSC Adv.*, 2013, **3**, 1486.